sciendo

Polish Journal of Chemical Technology, 26, 3, 56—62, 10.2478/pjct-2024-0030

Colorimetric detection of platinum (IV) ions based on triangular silver nanoprism particles in aqueous environmental sample

Jeong Won Ko[1], Se Hwan Park[2], and Weon Bae Ko[2, 3*]

[1]Department of Animal Resources Science, Chemistry Major, Sahmyook University, 815 Hwarang-ro, Nowon-gu, Seoul 01795, Republic of Korea
[2]Department of Convergence Science, Graduate School, Sahmyook University, 815 Hwarang-ro, Nowon-gu, Seoul 01795, Republic of Korea
[3]Department of Chemistry, Sahmyook University, 815 Hwarang-ro, Nowon-gu, Seoul 01795, Republic of Korea
[*]*Corresponding author: e-mail:* kowb@syu.ac.kr

Silver nitrate ($AgNO_3$), trisodium citrate dihydrate ($C_6H_5Na_3O_7 \cdot 2H_2O$), sodium borohydride ($NaBH_4$), and L-ascorbic acid ($C_6H_8O_6$) were combined in distilled water to create a triangular silver nanoprism particle (AgNPRP) solution. UV-visible (UV-vis) spectroscopy at wavelengths of 350–460 nm and 580–700 nm was observed, and as a result of them, the successful formation of the triangular AgNPRPs was confirmed. The prepared silver nanoprism particles were characterized by X-ray diffraction(XRD), X-ray photoelectron spectroscopy (XPS), scanning electron microscopy(SEM), and transmission electron microscopy(TEM) and employed for the colorimetric detection of platinum(IV) ions in an aqueous solution containing Pt^{4+} ions. The color of the aqueous silver nanoprism particle solution, containing Pt^{4+} ions, changed from blue to light brown before turning colorless. Using UV-vis spectrophotometry, the detection limit of the Pt^{4+} ion concentration was determined to be 6.23 μM in an aqueous solution of silver nanoprism particles. The proposed method was applied for detecting Pt^{4+} ions in tap water samples.

Keywords: colorimetric detection, detection limit, silver nanoprism particle, platinum (IV) ions.

INTRODUCTION

Owing to their importance in environmental protection, the selective recognition of heavy and transition metal ions has been an important topic of study attention during the last few decades[1–3]. One of these, platinum (Pt) ions, is extensively used in chemistry, especially in Pt-catalyzed processes that release a significant amount of Pt pollutants into the environment[4]. Therefore, it is necessary to quickly and easily monitor the presence of Pt species in the environment due to the sudden rise in Pt ion compounds and the toxicity associated with Pt ions[5].

With the widespread use of Pt (II) and Pt (IV) in chemical industries, an increasing number of platinum ions enter into the water system, which can potentially impact the environment and harm human health[6, 7]. Therefore, we must pay attention to the determination of Pt^{4+} ions as a trace element[8]. Traditional methods have been employed to detect platinum ions, including atomic absorption spectrometry (AAS)[9], spectrophotometry[10, 11], and inductively coupled plasma mass spectrometry (ICP-MS)[6, 12, 13]. Although these methods are accurate and sensitive, they require professional technicians or expensive instruments, and they are not suitable for field monitoring[5]. Therefore, more economical, selective, and rapid detection methods of platinum (IV) ions are necessary and are needed to gain qualitative and quantitative information for real-time analysis in analytical sciences[5, 14, 15].

Recently, nanomaterials have become popular in many fields because of their unique electronic, optical, magnetic, and photocatalytic properties[16]. Colorimetric detection methods based on nanomaterials have attracted great attention because of their distinctive advantages, such as simplicity and low cost[6, 17–21]. Moreover, the need for developing sensitive and selective sensors for the detection of low amounts of heavy metal ions from environmental samples has greatly increased[16, 22]. As a result, the approach presented in this study illustrates the colorimetric detection of Pt (IV) ions and can be used as a quick and portable test for the practical detection of Pt (IV) ions in an outdoor setting. The Pt (IV) ions can be found in wastes produced from mining facilities and mine leachates. During the dissolution process of the wastes including other metals, since oxidative reagents are used, Pt (IV) ion is favored in the leaching solutions[23]. Therefore, colorimetric detection of Pt(IV) ions is needed more than Pt(II) ions from these wastewater upon Pt(IV) detection compared to Pt(II) detection[24–26]. One of the promising application fields for triangular silver nanoprism particles (AgNPRPs) is the detection of metal ions for environmental monitoring[16]. Our group has developed a colorimetric detection method that uses triangular AgNPRPs to detect Pt (IV) ions in an aqueous solution.

MATERIALS AND METHODS

Materials

Calcium chloride dihydrate ($CaCl_2 \cdot 2H_2O$, ≥98%, EP) was supplied by DC Chemical Co. Ltd. Lead (II) nitrate ($Pb(NO_3)_2$, ≥99%, EP), manganese (II) sulfate monohydrate ($MnSO_4 \cdot H_2O$, ≥98%, EP), silver nitrate ($AgNO_3$, ≥99.8%, GR), and trisodium citrate dihydrate ($C_6H_5Na_3O_7 \cdot 2H_2O$, ≥99%, EP) were purchased from Samchun Chemicals. *L*-ascorbic acid ($C_6H_8O_6$, ≥99.5%, ACS), sodium borohydride ($NaBH_4$, ≥99%, Reagent plus), chloroplatinic acid hydrate ($H_2PtCl_6 \cdot xH_2O$, ≥99.9%,trace metals basis), copper chloride ($CuCl_2$, ≥99%, Reagent plus) and magnesium chloride hexahydrate ($MgCl_2 \cdot 6H_2O$, ≥99.5%, ACS) were purchased from Sigma-Aldrich.

Instruments

The crystal structure of the samples was analyzed by powder X-ray diffraction (XRD; Bruker, D8 Advanced, λ = 1.5418 Å) at 40 kV, 40 mA, with 2θ angles from 35 to 85°, and a scan rate of 0.2 sec/step at increments

of 0.02. The X-ray photoelectron spectroscopy (XPS) was utilized to evaluate the elemental composition and ionic states of the surface. (Thermo Fisher Scientific, NEXSA).The absorption spectra of the samples were recorded using a UV-vis spectrophotometer (Shimadzu UV-1691 PC). The surface morphologies of the samples were recorded using scanning electron microscopy (SEM; JEOL Ltd., JSM-6510) at an accelerating voltage of 10 kV. Transmission electron microscopy (TEM) and High--resolution transmission electron microscopy (HR-TEM; JEOL Ltd., NEO ARM) were carried out at an acceleration voltage of 100 kV-300 kV for the analysis of the morphology and crystallographic structure of the sample.

Preparation of triangular AgNPRP solution

In 20 mL of distilled water, 1.8 x 10^{-2} M silver nitrate ($AgNO_3$), 1.7 x 10^{-2} M trisodium citrate dihydrate ($C_6H_5Na_3O_7 \cdot 2H_2O$), and 0.05 x 10^{-2} M sodium borohydride ($NaBH_4$) solution were combined to create the seed solution. The growth solution was created by combining 20 mL of 1.7 x 10^{-1} M trisodium citrate dihydrate ($C_6H_5Na_3O_7 \cdot 2H_2O$) solution, 0.14 mL of 1.0 x 10^{-1} M silver nitrate ($AgNO_3$) solution, and 0.1 mL of 1.0 x 10^{-2} M *L*-ascorbic acid($C_6H_8O_6$) solution. Subsequently, 20 mL of the growth solution and 1.0 mL of the seed solution were mixed and agitated for 20 min to create the triangular AgNPRP solution[27].

Selective detection of Pt^{4+} ion in various metal cations using AgNPRP as a colorimetric detector

All the experiments were performed at room temperature. 150 μL of 14 ppm Pt^{4+} aqueous solution was added to 2500 μL of triangular AgNPRP solution. The mixed solution was stirred for 5 min. The selective detection of Pt^{4+} ion in aqueous triangular AgNPRP solution was investigated by naked eye and UV-vis absorption spectroscopy. Other ions, such as Ca^{2+}, Mg^{2+}, Pb^{2+}, Cu^{2+}, and Mn^{2+} were also tested in the same manner described above to confirm the selective detection of Pt^{4+} ions.

Detection of Pt^{4+} ions at various concentrations

The Pt^{4+} ion solutions were prepared at various concentrations ranging from 0 to 14 ppm. The above-mentioned 150 μL of each different concentration of Pt^{4+} ion solutions, which were each increased by 2 ppm, were added, respectively, to the vial containing 2500 μL of triangular AgNPRP solution. After the mixture was stirred for 5 min, the color change and detection of Pt^{4+} ions were monitored with the naked eye and UV-vis absorption spectroscopy.

Detection of Pt^{4+} ions in real tap water samples

Tap water collected in a part of Seoul was first filled using a filter paper with a pore size of 1 μm, and Pt^{4+} ion solutions, which have various concentrations from 0 to 14 ppm, were prepared in real tap water. 150 μL of each different concentration of Pt^{4+} ion solutions, which were each enhanced by 2 ppm, were then mixed with 2500 μL of aqueous triangular AgNPRP solution.

Subsequently, the color change and detection of Pt^{4+} ions were observed with the naked eye and UV-vis absorption spectroscopy.

RESULTS AND DISCUSSIONS

Characterization of triangular AgNPRPs

Figure 1 shows the UV–vis spectrum of the triangular AgNPRPs. The triangular AgNPRPs were successfully prepared, as indicated by the peaks at 350–460 nm and 580–700 nm[27]. The two peaks in the 350–460 nm and 580–700 nm ranges may be assigned to the in-plane quadrupole resonance and the in-plane dipole plasmon resonance of the triangular AgNPRPs, respectively. The in-plane quadrupole resonance was related to the width, and the in-plane dipole plasmon resonance was dependent on the edge length of triangular AgNPRPs.

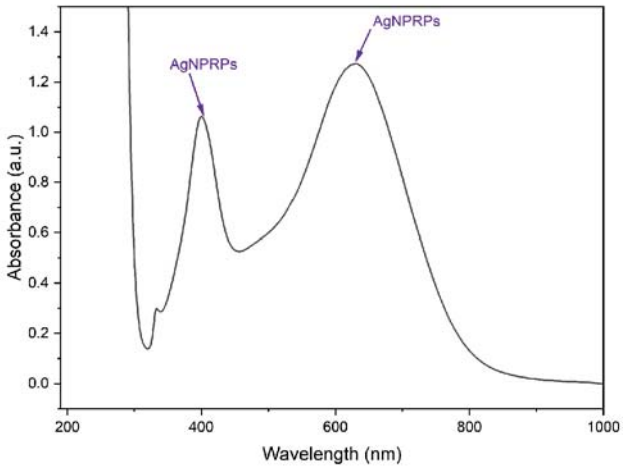

Figure 1. UV–vis spectrum of the triangular AgNPRPs

Powder XRD was used to investigate the crystal structure and crystallite size of the triangular AgNPRPs (Fig. 2). The peaks at 2θ = 38.14°, 44.20°, 64.57°, 77.49°, and 81.77° correspond to the (111), (200), (220), (311), and (222) planes of triangular AgNPRPs, respectively (JCPDS card No. 04-0783)[28]. In Fig. 2, the reflections present in the XRD pattern indicated crystal face-centered cubic (fcc) crystalline silver, respectively (JCPDS card No. 36-1451)[29]. According to the XRD results, triangular AgNPRPs were successfully synthesized. The crystallite size of the triangular AgNPRPs was determined using the Scherrer formula, $D = k \cdot \lambda/\beta \cdot \cos\theta$, where D is the crystallite size, λ is the wavelength of Cu-Kα radiation (taken as 0.154178 nm), *k* is the shape factor (taken as

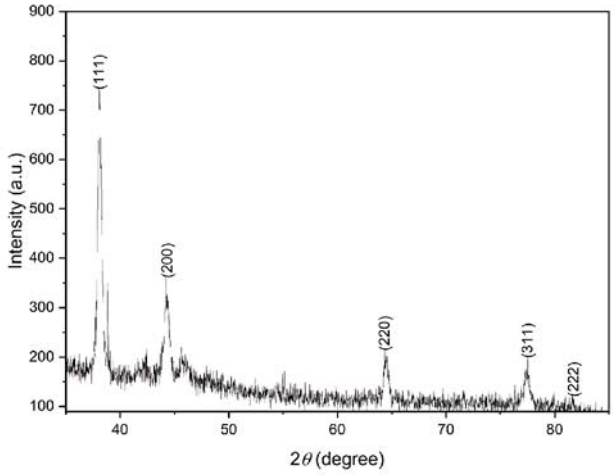

Figure 2. XRD pattern of the triangular AgNPRPs

Table 1. The average crystallite size of the triangular AgNPRPs estimated using the Scherrer equation. (AgNPRPs: Triangular silver nanoprism particles, FWHM: Full Width at Half Maximum)

Compound	Plane (h k l)	2 θ (degree)	FWHM (degree)	Crystallite size (nm)
AgNPRPs	111	38.14	0.45	19.49
	200	44.20	0.47	19.04
	220	64.57	0.53	18.51
	311	77.49	0.50	21.26
	222	81.77	0.47	23.34
Average				20.33

0.89), 2θ is the angle between the incident and scattered X-rays, and β is the full width at half maximum (FWHM). The average crystallite size of the triangular AgNPRPs was measured to be approximately 20.33 nm (Table 1).

An X-ray photoelectron spectroscopy (XPS) measurement was carried out to analyze the electron state of the Ag that exists within the triangular silver nanoprism. As shown in Fig. 3, two peaks were observed at 367.28 and 373.28 eV which are attributed to Ag $3d_{\frac{5}{2}}$ and Ag $3d_{\frac{3}{2}}$ of elemental silver in the triangular silver nanoprism[29, 30]. The splitting of the 3d doublet of Ag is 6.0 eV, indicating the presence of metallic Ag,

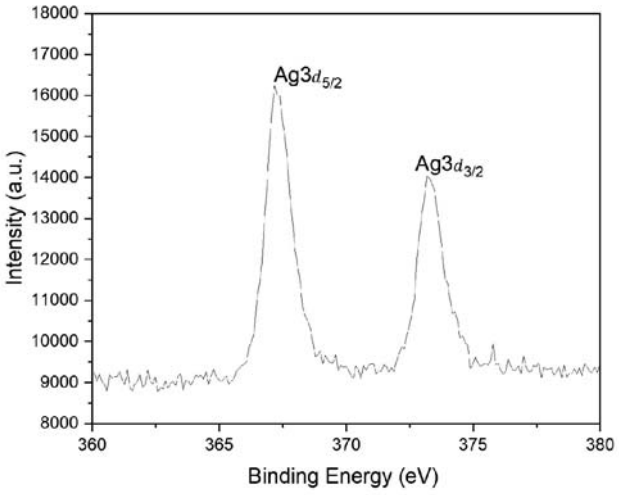

Figure 3. XPS spectrum of Ag 3d in the triangular Ag NPRPs

which provides strong evidence for the formation of a triangular silver nanoprism.

As shown in Fig. 4(a) and (b), transmission electron microscopy (TEM) measurements were carried out to characterize the morphology and particle size of the triangular Ag NPRPs. With TEM, the particle size is measured, whereas with XRD, it can be only measured the crystallite size, which is different from particle size. When the average crystallite size of the triangular Ag-NPRPs in Table 1 was compared to the particle size in Figure 4(a), the particle size has to be larger than crystallite size, because a particle can be constituted by several crystallites.

TEM images of Ag nanoparticles are presented in a triangular shape in Fig. 4 (a). HR-TEM image of an individual triangular AgNPRP in Fig. 4(b) shows that the nanoparticle is crystalline because the lattices of the Ag crystals can be observed. The lattice fringe spacing measurements indicate that the regular lattice spacing of d = 0.23 nm is consistent with the (111) plane in the face-centered cubic (fcc) structure of the Ag NPs[26].

Selectivity and sensitivity detection of Pt^{4+} ions

As shown in Fig. 5(a) and (b), for the triangular AgNPRP selective colorimetric detection of metal ions, different metal cations such as Pt^{4+}, Ca^{2+}, Mg^{2+}, Pb^{2+}, Cu^{2+}, and Mn^{2+}, were initially screened by exposing the colloidal AgNPRP solution to each of these metal ions (14 ppm) and visually monitoring the color change in solution.(Fig. 5(a)). Only the color of the AgNPRP solution after Pt^{4+} ions were added, changed from blue to colorless, as shown in Fig. 5(a) and Table 2.

Table 2. Color change of various metal ions using triangular AgNPRP solution

Metal ions	Color change (Y/N)
Ca^{2+}	No
Mg^{2+}	No
Pb^{2+}	No
Cu^{2+}	No
Mn^{2+}	No
Pt^{4+}	Yes (Blue to colorless)

Fig. 5(b) showed that the optical absorbance spectra of AgNPRP solution and each sample contained in different kind of metal cations such as Pt^{4+}, Ca^{2+}, Mg^{2+}, Pb^{2+}, Cu^{2+}, and Mn^{2} ions with AgNPRP colorimetric probe. The location of the surface plasmon resonance

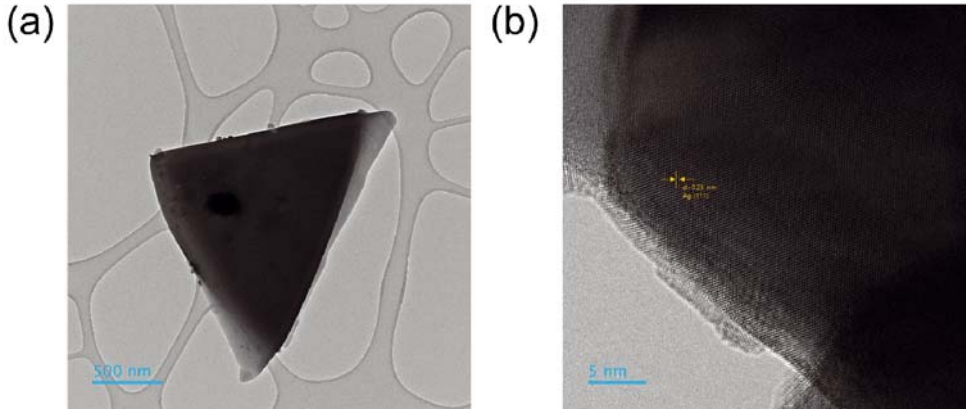

Figure 4. Typical TEM image (a) and HRTEM image (b) of triangular Ag NPRPs

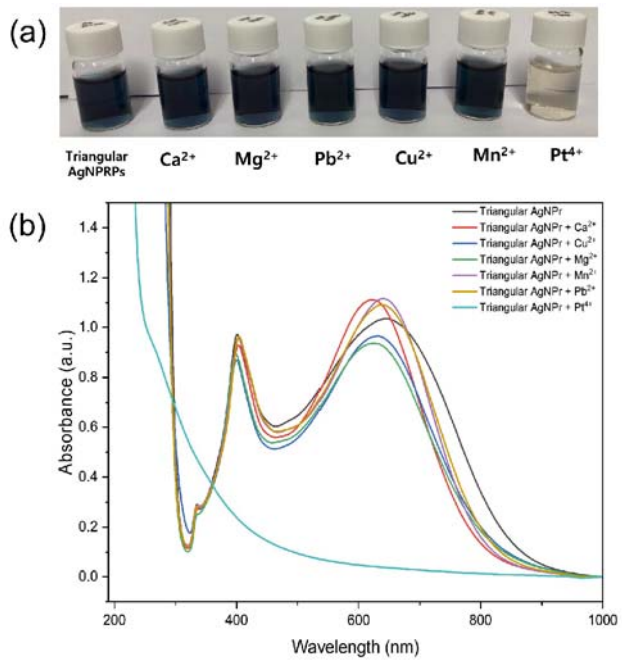

Figure 5. (a) Visual color change, and (b) UV-vis absorption spectra showing SPR peaks of triangular AgNPRPs and shifts for detection upon addition of different metal ions (Pt^{4+}, Ca^{2+}, Mg^{2+}, Pb^{2+}, Cu^{2+}, and Mn^{2+})

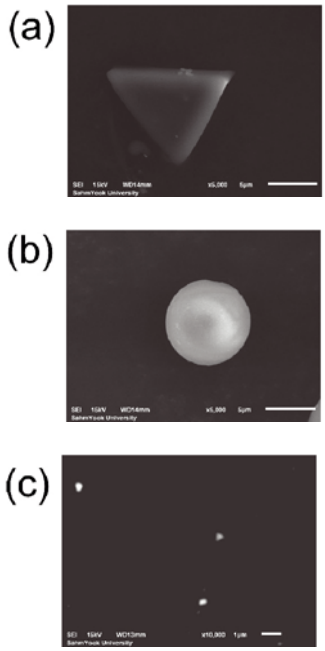

Figure 6. SEM image for triangular AgNPRPs (a) in the absence of Pt^{4+} ions, (b) in the presence of Pt^{4+} ions, and (c) the approximate yield of AgNPRPs

(SPR) peak shift of various metal cations did not change, except for Pt^{4+} ions[31]. This indicates that Pt^{4+} ion is selective for the AgNPRP solution. Also, the colorimetric detection of Pt^{4+} ions and various metal ions in several different water samples based on triangular AgNPRP was compared with previous research findings in Table 3[32–35].

Fig. 6 shows the morphological surface changes of the Ag nanoparticles (NPs) before and after the addition of Pt^{4+} ions. When Pt^{4+} ions were absent, the Ag NPs in Fig. 6(a) exhibited a triangular prism shape. In contrast, it can be observed from Fig. 6(b) that the Ag NPs exhibited a spherical shape after Pt^{4+} ions were added. These results indicated that the chemical reaction may proceed

Table 3. Comparison of colorimetric detection conditions of ions based on triangular silver nanoprism particles with other studies

Detection metal ion	Sample	Limit of detection (μM)	References
Ba^{2+}	Tap water	74	32
Cr^{2+}	River water	3.6×10^{-3}	33
Ni^{2+}	Real water, Lake water	0.05	34
Hg^{2+}	Tap water, Drinking water, Lake water	0.03	35
Pt^{4+}	Tap water	6.23	This work

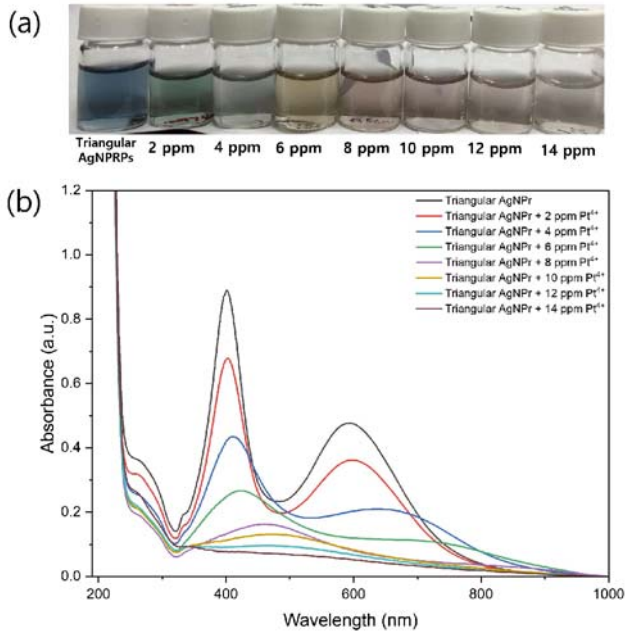

Figure 7. (a) Visual color change, and (b) UV-vis absorption spectra for detection of Pt^{4+} ions at various concentrations from 0 to 14 ppm in triangular AgNPRPs solution

according to the change in the shape of the Ag NPs with the addition of the Pt^{4+} ion solution. In Fig. 6(c), by observing the image of the scanning electron microscope (SEM) of the synthesized AgNPRPs, it may be that the approximate yield of AgNPRPs was about 66%.

The sensitivity of the colorimetric detection of Pt^{4+} ions with triangular AgNPRPs was investigated using both the colorimetric response (Fig. 7(a)) and UV-vis spectra (Fig. 7(b)). The photographic image of the triangular AgNPRP solution color varied depend on the with Pt^{4+} ion concentrations (0-14 ppm), as shown in Fig. 7(a). The color change of the triangular AgNPRP solution as the concentration of Pt^{4+} ions increased to approximately 14 ppm could be observed to become colorless when compared to the control (without Pt^{4+}); however, the color change of the triangular AgNPRP solution could not be observed at 2 ppm, the concentration of Pt^{4+} ions in Fig. 7(a).

Fig. 7(b) showed that the optical absorbance spectra of the triangular AgNPRP solution and distilled water sample contained different concentrations of Pt^{4+} ion used on AgNPRP colorimetric probe. According to increasing the concentration of Pt^{4+} ion, the peaks were

disappeared between 580–700 nm and the peaks intensity between 350–460 nm decreased.

Detection of Pt $^{4+}$ ions in real water samples

For the quantitative detection of Pt^{4+} ions in actual water samples, the potential efficacy of the triangular AgNPRP for the Pt^{4+} detection test was further expanded and proven in tap water[36]. Fig. 8(a) shows photograph of the AgNPRP-based colorimetric probe for real-time detection of Pt^{4+} ions in tap water at various concentrations ranging from 0 to 14 ppm.

The color of solution in the bottle changed from blue to light brown before turning colorless. The results in Fig. 8(a) indicated that AgNPRP-based colorimetric probe exhibited excellent sensitivity at a concentration of 14 ppm for Pt^{4+} ions in tap water. These results indicated that AgNPRP based colorimetric probe can be used for detection of Pt^{4+} ion in real tap water samples. Fig. 8(b) showed that the optical absorbance spectra of the AgNPRP solution and tap water samples containing various concentrations of Pt^{4+} ion used in the AgNPRP colorimetric probe. As the concentration of Pt^{4+} ions increased from 0 to 14 ppm, the peaks between 580–700 nm faded, and the intensity between 350–460 nm diminished. The limit of detection (LOD) is one of the key characteristics for validating the effectiveness of a sensing probe[37]. Figure 9 illustrates the linear relationship between the difference of absorbance intensity (Δ a) and

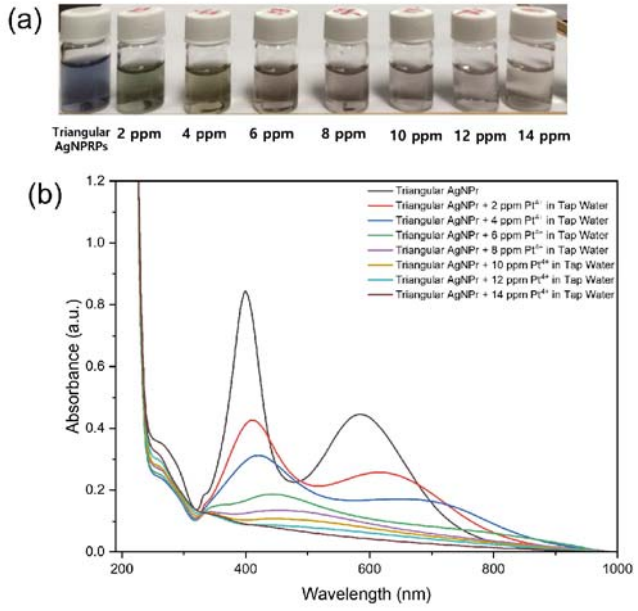

Figure 8. (a) Visual color change, and (b) plot of optical absorbance for various concentrations (0–14 ppm) of Pt^{4+} ions in real tap water samples

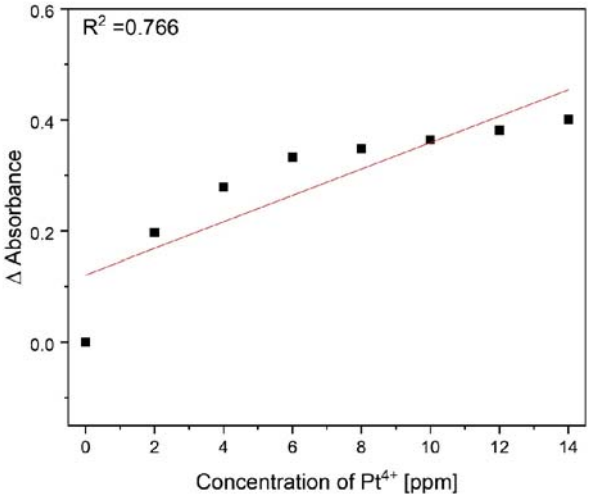

Figure 9. Linear plot absorbance intensity difference at wavelength 585 nm towards Pt^{4+} ions concentration

Pt^{4+} ion concentration (ppm), represented by the equation $y = 0.0238$ x, where 'y' and 'x' to the Pt^{4+} ion concentration. The absorbance intensity difference showed linearly with the increasing concentration of Pt^{4+} ranging from 0 to 14 ppm. The LOD for Pt^{4+} ions, determined using the developed sensing probe, was approximately 6.23 μM. It was calculated by LOD=3.3 X (σ/s), where σ is the standard deviation of the sample, s is the linear plot's slop, resulting in 3.3 X (0.0448/0.0238) equal to 6.23 μM. The linear regression coefficient (R^2) of 0.766 was obtained for the concentration of Pt^{4+} ranging from 0 to 14 ppm. The limits of detection of various metal ions using AgNPRPs are compared in Table 3.

The colorimetric detection mechanism of Pt^{4+} ions using triangular AgNPRPs

Ascorbic acid and trisodium citrate are responsible for reducing Ag^{1+} to Ag(0) and forming AgNPRPs[38]. Additionally, these reductants serve as capping agents for the stability of AgNPRP. Furthermore, the Pt^{4+} ion has a higher reduction potential than Ag^{1+}, resulting in a spontaneous redox reaction of $4Ag + 2Pt^{4+} \rightarrow 4Ag^{+} + Pt_2^{2+}$.

Oxidation of Ag^0 to Ag^{1+} changes from blue to colorless, which means that the triangular AgNPRPs (blue) changes into Ag^{1+} ions (colorless) as was seen when the colorless $AgNO_3$ was put in an aqueous solution. This redox reaction is the basis for colorimetric detection of Pt^{4+} ions by triangular AgNPRPs. Most transition metals, alkali metals, and alkaline earth metals have lower reduction potentials than Ag^{1+}, which prevents them from oxidizing Ag^0 of AgNPs to Ag^{1+} ion, but the Pt^{4+}

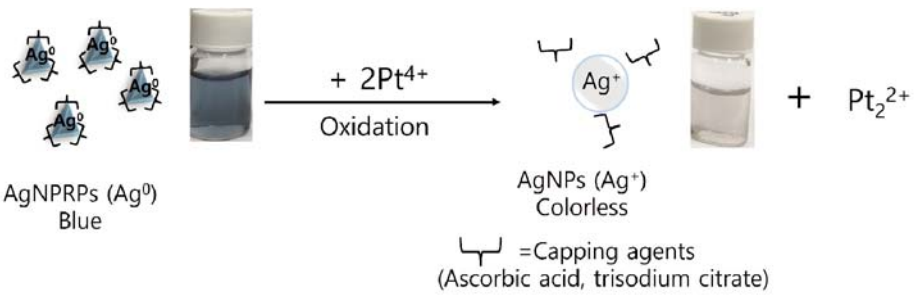

Figure 10. Colorimetric detection mechanism for Pt^{4+} ions using triangular AgNPRPs via redox reactions, as proposed schematically

ion has a higher reduction potential than Ag^{1+}, thus allowing for highly selective Pt^{4+} ion analysis. We suggest a mechanism shown in Fig. 10 for Pt^{4+} colorimetric detection by redox reaction in the mixture based on this reduction potential chemistry. In addition, Pt^{4+} ion has a higher reduction potential than Ag^{+} ion, and thus Pt^{4+} ion can be changed Ag^{0} of AgNPRPs into Ag^{1+} ion. The role of triangular AgNPRPs is as an oxidation agent in detecting Pt^{4+} ions in tap water samples.

CONCLUSIONS

The triangular AgNPRPs were characterized by X-ray diffraction (XRD), X-ray photoelectron spectroscopy (XPS), scanning electron microscopy (SEM), transmission electron microscopy (TEM), high-resolution transmission electron microscopy (HR-TEM) and UV-vis spectroscopy which were employed for colorimetric detection of Pt^{4+} ions in an aqueous solution containing Pt^{4+} ions.

There are multiple benefits associated with this approach for the Pt^{4+} ions detection method.

First, using triangular AgNPRPs in an aqueous sample, this approach could be used to monitor Pt^{4+} ions by colorimetric detection.

Second, this method simplifies operations and lowers analytical costs because it does not require complicated or expensive instruments. Third, this method can be used directly without modification. Fourth, this technique facilitates the colorimetric detection of concentrations as low as 6.23 μM by UV-vis spectroscopy and allows for the rapid and sensitive detection of Pt^{4+} ion.

Lastly, this method exhibits good sensitivity for Pt^{4} ions, regardless of the various metal ions already present in the aqueous solution. The future direction and perspectives for this potential of triangular AgNPRPs for detecting Pt^{4+} ions in tap water samples may be used in the application of the probe to sense Pt^{4+} ions in biological and environmental samples.

ACKNOWLEDGEMENT

This study was supported by research funding from Sahmyook University, South Korea.

LITERATURE CITED

1. Kim, H.N., Ren, W.X., Kim, J.S. & Yoon, J. (2012). Fluorescent and colorimetric sensors for detection of lead, cadmium, and mercury ions. *Chem. Soc. Rev.* 41, 3210e3244. DOI: 10.1039/C1CS15245A.

2. Li, J., Wang, X.X., Zhao, G.X., Chen, C.L., Chai, Z.F., Alsaedi, A., Hayat, T. & Wang, X.K. (2018). Metal-organic framework-based materials: superior adsorbents for the capture of toxic and radioactive metal ions. *Chem. Soc. Rev.* 47, 2322e2356. DOI: 10.1039/C7CS00543A.

3. Amin, N., Siddiqi, H.M., Lin, Y.K., Hussain, Z. & Majeed, N. (2020). Bovine serum albumin protein-based liquid crystal biosensors for optical detection of toxic heavy metals in water. *Sensors,* 20, 298. DOI: 10.3390/s20010298.

4. Lin, L., Yao, S., Gao, R., Liang, X., Yu, Q., Deng, Y., Liu, J., Peng, M., Jiang, Z., Li, S., Li, Y-W., Wen, X-D., Zhou, W. & Ma, D. (2019). A highly CO-tolerant atomically dispersed Pt catalyst for chemoselective hydrogenation. *Nat. Nanotechnol.* 14, 354–361. DOI: 10.1038/s41565-019-0366-5.

5. Feng, W., Zengji, Z., Testoff, T.T., Wang, T., Yan, X., Li, X., Liu, D., Lichang Wang, L. & Zhou, X. (2021). Photoinduced charge-separated molecular probe for ultrasensitive spectrum analysis and rapid colorimetric detection of platinum ions. *Anal. Chim. Acta*, 1153, DOI: 10.1016/j.aca.2021.338278.

6. Sang, F., Liu, J., Zhang, X. & Pan, J. (2018). An aptamer-based colorimetric Pt(II) assay based on the use of gold nanoparticles and a cationic polymer. *Microchim. Acta*, 185, 267. DOI: 10.1007/s00604-018-2794-6.

7. Rudolph, E., Hann, S., Stingeder, G. & Reiter, C. (2005). Ultra-trace analysis of platinum in human tissue samples. *Anal. Bioanal. Chem.* 382, 1500–1506. DOI: 10.1007/s00216-005-33706.

8. Chen, L., Fu, X., Lu, W. & Chen, L. (2013). Highly sensitive and selective colorimetric sensing of Hg^{2+} based on the morphology transition of silver nanoprisms. *ACS Appl. Mater. Interfaces*, 5, 284–290. DOI: 10.1021/am3020857.

9. Brouwers, E.E., Tibben, M.M., Joerger, M., Van, T.O., Rosing, H., Schellens, J.H.M. & Beijnen, J.H. (2005). Determination of oxaliplatin in human plasma and plasma ultrafiltrate by graphite-furnace atomic-absorption spectrometry. *Anal. Bioanal. Chem.* 382, 1484–1490. DOI: 10.1007/s00216-005-3302-5.

10. Huang, Z., Timerbaev, A.R., Keppler, B.K. & Hirokawa, T. (2006). Determination of cisplatin and its hydrolytic metabolite in human serum by capillary electrophoresis techniques. *J. Chromatogr. A.* 1106, 75–79. DOI: 10.1016/j.chroma.2005.09.042.

11. Yang, H., Cui, H., Wang, L., Yan, L., Qian, Y., Zheng, X.E, Wei, W. & Zhao, J. (2014). A label-free G-quadruplex DNA-based fluorescence method for highly sensitive, direct detection of cisplatin. *Sens. Actuators B Chem.* 202, 714–720. DOI: 10.1016/j.snb.2014.05.027.

12. Martinčič, A., Cemazar, M., Sersa, G., Kovač, V., Milačič, R. & Ščančar, J. (2013). A novel method for speciation of Pt in human serum incubated with cisplatin, oxaliplatin and carboplatin by conjoint liquid chromatography on monolithic disks with UV and ICP-MS detection. *Talanta,* 213, 141–148. DOI: 10.1016/j.talanta.2013.05.016.

13. Yaroshenko, D.V., Grigoriev, A.V., Sidorova, A.A. & Kartsova, L.A. (2013). Determination of cisplatin in blood plasma by liquid chromatography with mass spectrometry detection. *J. Anal. Chem.* 68, 156–160. DOI: 10.1134/S1061934813020160.

14. Pershagen, E., Nordholm, J. & Borbas, K.E. (2012). Luminescent lanthanide complexes with analyte-triggered antenna formation. *J. Am. Chem. Soc.* 134, 9832e9835. DOI: 10.1021/ja3004045.

15. Dhanushkodi, M., Kumar, G.G.V., Balachandar, B.K., Sarveswari, S., Gandhi, S. & Rajesh, J. (2020). A simple pyrazine based ratiometric fluorescent sensor for Ni2þ ion detection. *Dyes Pigm.* 173, 107897. DOI: 10.1016/j.dyepig.2019.107897.

16. Prosposito, P., Mochi, F., Ciotta, E., Casalboni, M., De Matteis, F., Venditti, I., Fontana, L., Testa, G. & Fratoddi, I. (2016). Hydrophilic silver nanoparticles with tunable optical properties: Application for the detection of heavy metals in water. *Beilstein J. Nanotechnol.* 7(1), 1654–1661. DOI: 10.3762/bjnano.7.157.

17. Niu, S., Lv, Z., Liu, J., Bai, W., Yang, S. & Chen, A. (2014). Colorimetric aptasensor using unmodified gold nanoparticles for homogeneous multiplex detection. *PLoS One.* 9(10): e109263. DOI: 10.1371/journal.pone.0109263.

18. Sang, F., Li, X., Zhang, Z., Liu, J. & Chen, G. (2017). Recyclable colorimetric sensor of Cr^{3+} and Pb^{2+} ions simultaneously using a zwitterionic amino acid modified gold nanoparticles. *Spectrochim. Acta A*, 193, 109–116. DOI: 10.1016/j.saa.2017.11.048.

19. Zhang, Y., Li, R., Xue, Q., Li, H. & Liu, J. (2015). Colorimetric determination of copper(II) using a polyamine-functionalized gold nanoparticle probe. *Microchim. Acta.* 182, 1677–1683. DOI: 10.1007/s00604-015-1498-4.

20. He, Y., Cheng, F., Pang, D.W. & Tang, H.W. (2016). Colorimetric and visual determination of DNase I activity using gold nanoparticles as an indicator. *Microchim. Acta.* 184, 1–6. DOI: 10.1007/s00604-016-2003-4.

21. Du, G., Zhang, D., Xia, B., Xu, L., Wu, S., Zhan, S., Ni, X., Zhou, X. & Wang, L. (2016). A label-free colorimetric

progesterone aptasensor based on the aggregation of gold nanoparticles. *Microchim. Acta.* 183, 2251–2258. DOI: 10.1007/s00604-016-1861-0.

22. Ban, D.K., Pratihar, S.K. & Paul, S. (2015). Controlled modification of starch in the synthesis of gold nanoparticles with tunable optical properties and their application in heavy metal sensing. *RSC Adv.* 5, 81554–81564. DOI: 10.1039/C5RA16473G.

23. Boudesocque, S., Mohamadou, A., Conreux, A., Marin, B. & Dupont, L. (2019). The recovery and selective extraction of gold and platinum by novel ionic liquids. *Sep. Purif. Technol.* 210, 824–834. DOI: 10.1016/j.seppur.2018.09.002.

24. Mosai, A.K., Chimuka, L., Cukrowska, E.M., Kotzé, I.A. & Tutu, H. (2021). Batch and flow-through column adsorption study: recovery of Pt^{4+} from aqueous solutions by 3-aminopropyl (diethoxy) methylsilane functionalised zeolite (APDEMSFZ). *Environ. Dev. Sustain.* 23, 7041–7062. DOI: 10.1007/s10668-020-00903-x.

25. Park, H.N., Choi, H.A. & Won, S.W. (2018). Fibrous polyethylenimine/polyvinyl chloride crosslinked adsorbent for the recovery of Pt (IV) from acidic solution: Adsorption, desorption and reuse performances. *J. Clean. Prod.*176, 360–369. DOI: 10.1016/j.jclepro.2017.12.160.

26. Bilgin, F. & Imamoglu, M. (2024). Effect of spacer length between N atoms of linear alkyl triamines on adsorption of anionic platinum (IV) ions. *Desalin. Water Treat.* 317, 100229. DOI: 10.1016/j.dwt.2024.100229.

27. Roh, J., Park, E.J., Park, K., Yi, J. & Kim, Y. (2010). Fast preparation of citrate-stabilized silver nanoplates and its nanotoxicity. *Korean J. Chem. Eng.* 27, 1897–1900. DOI: 10.1007/s11814-010-0299-z.

28.Yang, J., Zheng, H., Han, S., Jiang, Z. & Chen, X. (2015). The synthesis of nano-silver/sodium alginate composites and their antibacterial properties. *RSC Adv.* 5, 2378–2382. DOI: 10.1039/C4RA12836B.

29. Li, Y., Ye, Y., Fan, Y., Zhou, J., Jia, L., Tang, B. & Wang, X. (2017) Silver Nanoprism-Loaded Eggshell Membrane: A Facile Platform for In Situ SERS Monitoring of Catalytic Reactions. *Crystals*. 7, 45. DOI: 10.3390/cryst7020045.

30. Liang, M., Su, R., Huang, R., Qi, W., Yu, Y., Wang, L. & He, Z. (2014). Facile in situ synthesis of silver nanoparticles on procyanidin-grafted eggshell membrane and their catalytic properties. *ACS Appl. Mater. Interfaces*, 6(7), 4638–4649. DOI: 10.1021/am500665p.

31. Desai, M.P., Patil, R.V. & Pawar K.D. (2020). Selective and sensitive colorimetric detection of platinum using *Pseudomonas stutzeri* mediated optimally synthesized antibacterial silver nanoparticles. *Biotechnol. Rep.* 25, e00404. DOI: 10.1016/j.btre.2019.e00404.

32. Ardianrama, A.D., Pradyasti, A., Woo, H.C. & Kim, M.H. (2020). Colorimetric sensing of barium ion in water based on polyelectrolyte-induced chemical etching of silver nanoprisms. *Dyes Pigm.* 181, 108578. DOI: 10.1016/j.dyepig.2020.108578.

33. Pu, Z.F.,Wu, B.C., Tan, Y.H., Wen, Q.L., Ling, J., & Cao Q. E. (2021). Selective Aggregation of Silver Nanoprisms Induced by Monohydrogen Phosphate and its Application for Colorimetric Detection of Chromium (III) Ions. *J. Anal. Test.* 5, 225–234. DOI: 10.1007/s41664-021-00183-y.

34. Chen, N., Zhang, Y., Liu, H., Ruan, H., Dong, C., Shen, Z. & Wu, A. (2016). A supersensitive probe for rapid colorimetric detection of nickel ion based on a sensing mechanism of anti-etching. *ACS Sustain. Chem. Eng.* 4, 6509–6516. DOI: 10.1021/acssuschemeng.6b01326.

35. Chen, N., Zhang, Y., Liu, H., Wu, X., Li, Y., Miao, L., Shen, Z. & Wu, A. (2016). High-performance colorimetric detection of Hg^{2+} based on triangular silver nanoprisms. *ACS Sens.,* 1, 521–527. DOI: 10.1021/acssensors.6b00001.

36. Chen, N., Zhang, Y., Liu, H., Wu, X., Li, Y., Miao, L., Shen, Z. & Wu, A. (2016). High-prformance colorimetric detection of Hg^{2+} based on triangular silver nanoprisms. *ACS Sens.,* 2016, 1:521–527. DOI: 10.1021/acssensors.6b00001.

37. Hastuti, F.W. & Kim, M.H. (2024). Silver nanoprism-mediated colourimetric sensing probe for efficient detection of Pd (II) and Pt (II) ions in water and reuse of formed bimetallic nanoprisms. Spectrochim. *Acta Part A: Molec. Biomolec. Spectros*. 124234. 10.1016/j.saa.2024.124234.

38. Firdaus, M.L., Fitriani, I., Wyantuti, S., Hartati, Y.W., Khaydarov, R., Mcalister, J.A., Obata, H. & Gamo, T. (2017). Colorimetric detection of mercury(II) ion in aqueous solution using silver nanoparicles. *Anal. Sci.* 33, 831– 837. DOI: 10.2116/analsci.33.831.